Eletrônica de Potência
Open Journal of Power Electronics

Received July 30, 2024; accepted November 13, 2024; Date of publication December 04, 2024.
The review of this paper was arranged by Associate Editor Victor F. Mendes and Editor-in-Chief Heverton A. Pereira.

Digital Object Identifier http://doi.org/10.18618/REP.e202453

Ancillary Services to Mitigate Non-linear and Unbalanced Load Based on CPT Using a DFIG Power Plant

Carlos Leonardo A. Hinostroza[1], João Pedro C. Silveira[1], Marcelo Vinicius de Paula[2], Pedro José dos Santos Neto[2], Ernesto Ruppert Filho[1], Tárcio André S. Barros[1]

[1]Universidade Estadual de Campinas, Faculdade de Engenharia Elétrica e de Computação, Campinas - SP, Brazil.
[2]Universidade Estadual de Campinas, Faculdade de Engenharia Mecânica, Campinas - SP, Brazil.

e-mail: car.ancasi.h@gmail.com; jpedro.carvalhosilveira@gmail.com; mvpaula@unicamp.br; pedrosn@unicamp.br; ruppert@unicamp.br; tarcio87@unicamp.br.

ABSTRACT The increase of renewable energy sources and non-linear loads on the utility grid introduces challenges in maintaining the nominal conditions of the utility grid. A viable approach to addressing some of these challenges is to utilize renewable energy conversion systems that accomplish supplementary functions in addition to supplying active power. This paper presents the implementation of ancillary services to mitigate non-linear and unbalanced loads using a single Doubly Fed Induction Generation (DFIG) power plant. For this, the Conservative Power Theory (CPT) is used to provide three types of services simultaneously: active filtering, reactive power compensation, and unbalanced phase compensation. A back-to-back converter is used to control the power flow in the DFIG and employ ancillary services. Two control strategies are compared: in the dq reference frame and the $\alpha\beta$ reference frame. Simulations in MatLab/Simulink are used to evaluate the response of the CPT and the control strategies. The ancillary services performance is analyzed using the indicator based on standards and CPT factor. The results show that the indicators comply with the standards depending on the active power supply. Moreover, $\alpha\beta$ reference frame exhibits better performance than dq reference frame.

KEYWORDS Ancillary services, conservative power theory, doubly fed induction generator, wind energy conversion system.

I. INTRODUCTION

Ancillary services can be incorporated into converters from renewable energy sources, such as wind and solar, which are connected to the utility grid [1]–[4]. For Wind Energy Conversion System (WECS) using the DFIG, it is possible to include reactive power control, fault/voltage ride through, power quality improvement, frequency control, and power oscillation damping, thus improving the power quality in the power grid [3].

The active filtering can be added in DFIG converters control to mitigate harmonics through the Point of Common Coupling (PCC) current [5]–[7]. In [5], the researches compare control strategies in the synchronous reference frame applied to the Rotor Side Converter (RSC), the Grid Side Converter (GSC), and a combination of both converters to mitigate current harmonics in the PCC current. The authors from [6] add active filtering to the RSC, which extracts maximum wind energy through an MPPT. Meanwhile, in [7] and [8], the GSC is used to provide ancillary services in the dq and $\alpha\beta$ reference frames. In [9], active filtering is added to the GSC, which utilizes direct power control. The ancillary active filtering service needs to identify the harmonic spectrum that will be mitigated. The authors from [6], [10] and [9] employ a harmonic identifier based on instantaneous power theory. The harmonic identification method in the synchronous reference frame is employed in [5] and [11]. In [8], the author analyzes control strategies employing different harmonic identifiers to mitigate harmonics in a non-linear electrical load. In [12], active filtering mitigates the 5^{th} and 7^{th} order harmonics by employing a highly selective filter to identify these harmonics. The authors from [7] and [13] employs conservative power theory to identify harmonics in the non-linear electrical load.

The DFIG reactive power can be controlled through converters such as RSC and GSC [3]. In [6], active power compensation is accomplished in the RSC. Such paper proposes a management of the functions of active power compensation and harmonic current mitigation in the PCC. In [14], the RSC injects current into the utility grid to maintain the unity power factor, while the GSC compensates for the reactive power of the non-linear load. In [15], the GSC regulates electrical powers using a fuzzy logic controller and a hysteresis current controller.

The research papers [11], [16], [14] and [17] demonstrate wind systems with DFIG connected to non-linear and unbalanced loads. In [14], the GSC presents a hysteresis-based control that compensates for harmonics and reactive power of the unbalanced non-linear load. However, no indicator is used to analyze the unbalanced phase. In [16], the author employs the GSC to compensate for unbalanced phase current, characterizing the unbalanced non-linear electrical load through conservative power theory. The strategy proposed in [5] was analyzed in [17] for non-linear and unbalanced electrical loads, improving harmonic distortion and unbalanced phase indicators. In [11] and [17], the research utilizes the phase unbalance indicator calculated as the maximum variation of a phase current concerning the average of the three phases, but limit for this indicator is not considered.

In this context, the DFIG power plants incorporate an ancillary service in the back-to-back converter control to mitigate an undesirable condition of the utility grid. Thus, the present paper is focused on three types of ancillary services to mitigate the non-linear and unbalanced loads using a single DFIG power plant. For this, the Conservative Power Theory (CPT) is used to provide three types of services simultaneously: active filtering, reactive power compensation, and unbalanced phase compensation. The indicators used to evaluate the ancillary services, considering PRODIST and IEEE standards, are discussed. The simulation results provided these standard indicators as well as CPT indicators. Additionally, two control strategies in the dq reference frame and $\alpha\beta$ reference frame used in back-to-back converter are compared. This paper is an extension of the proposed system presented in the conference paper [7]. The main contributions of this paper in relation to [7] are as follows:

- The proposed system mitigates the non-linear and unbalanced loads.
- Comparison of two control strategies for providing three types of ancillary services simultaneously.
- Discussion about the standard indicators and CPT indicators to evaluate the ancillary services.

The rest of the paper is outlined as follows. Section 2 describes the DFIG and non-linear and unbalanced load connected in PCC. Section 3 approaches the RSC and GSC control. Section 4 details the CPT and the application for ancillary services. Section 5 discusses the standard and CPT indicators. Section 6 shows and discusses the results. Finally, section 7 presents the conclusions.

II. DFIG POWER PLANT

A. DFIG

The DFIG is one of the most frequently employed solutions in WECS. This generator is composed of stator windings and rotor windings. The stator windings of the DFIG are directly connected to the utility grid, while the rotor windings are connected to the back-to-back converter, as shown in Fig. 1. The back-to-back converter is composed of two three-phase VSI converters: the RSC, which is connected to the rotor windings, and the GSC, which is connected to the utility grid. In this configuration, the current waveform supplying the rotor windings is freely controlled [18]. The mathematical model of DFIG is expressed in the synchronous reference frame for the control design, as shown in (1) to (5).

$$v_{dqs} = \frac{d\psi_{dqs}}{dt} + j\omega_e\psi_{dqs} + r_s i_{dqs} \quad (1)$$

$$v'_{dqr} = \frac{d\psi'_{dqr}}{dt} + j\left(\omega_e - \omega_r\right)\psi'_{dqr} + r'_r i'_{dqr} \quad (2)$$

$$\psi_{dqs} = L_s i_{dqs} + L_m i'_{dqr} \quad (3)$$

$$\psi'_{dqr} = L_r i'_{dqr} + L_m i_{dqs} \quad (4)$$

$$\omega_r = \frac{p}{2}\omega_m \quad (5)$$

where dq indexes refer to the complex variable by dq reference frame components. s and r indexes refer to the stator and rotor variables, respectively. The variables v, i, r, and L are voltage, current, resistance, and inductance, respectively. L_m is mutual inductance. ψ is magnetic flux. ω_m and ω_r are the mechanical angular speed and electrical angular frequency of the rotor, respectively. ω_e is the electrical angular frequency of the stator. The number of poles is p.

The electromagnetic power represents the combined active power of the stator (P_s) and rotor (P_r), excluding power losses. The rotor active power is a fraction of the stator active power according to slip ratio s_l, as expressed in (6). Thus, the rotor speed varies active power through the rotor.

$$P_r \approx -s_l P_s \quad (6)$$

Wind systems operate within a wind speed range. In this operational range, the turbine speed is regulated according to wind speed to maximize output power. In DFIG systems, the slip rate typically ranges from -0.3 to 0.3, ensuring maximum output power for the operational range. For this reason, the rated power of the back-to-back converter is normally only $30\,\%$ of the DFIG's rated power [18]. In WECS simulation, the slip rate reaches its range limits for the back-to-back converter to operate near its power rating.

B. Non-linear and unbalanced load

The composition of the electrical load used in this work is shown in Table 1. These loads contribute to the current profile with harmonic content, reactive power consumption, and unbalanced phase current.

III. DFIG CONTROL

A. RSC Control

The RSC control uses the stator flux-oriented concept, allowing the rotor current to regulate the active and reactive power through the DFIG stator. Assuming stator resistance is close to zero, the dq reference currents are given as functions

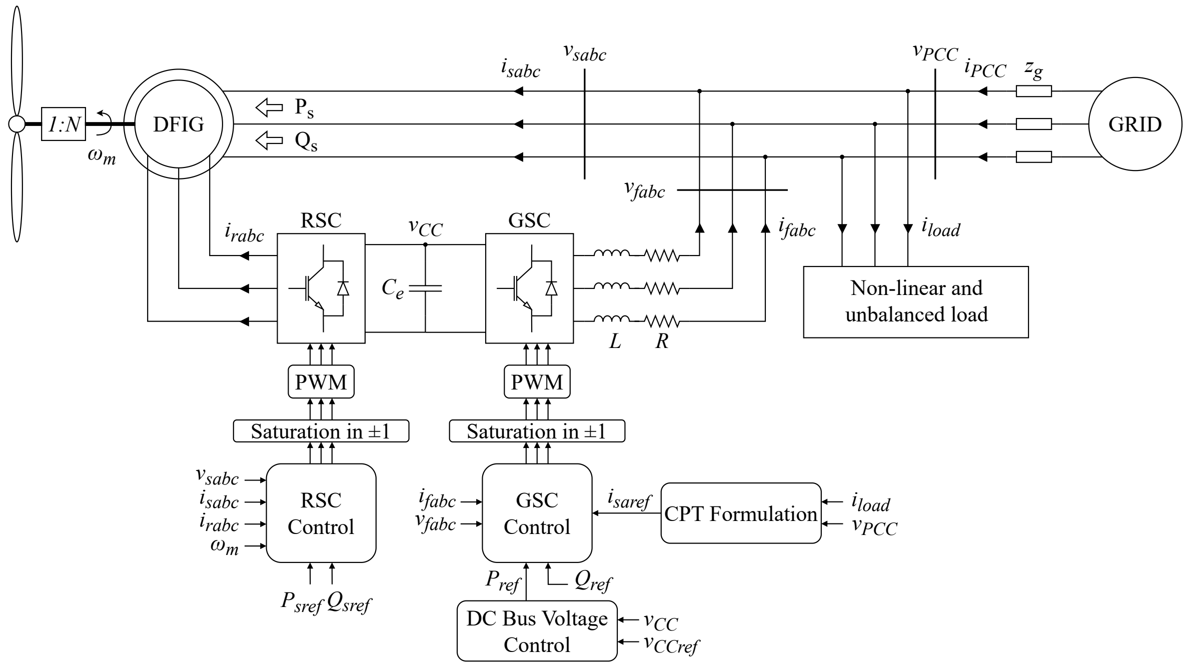

FIGURE 1. Schematic of WECS with DFIG generator and, non-linear and unbalanced load.

TABLE 1. Active and reactive of electrical loads.

Electrical load	Active power	Reactive power
Controlled three-phase rectifiers	70 kW	60 kVAR
Three-phase diode rectifiers	1 MW	84 kVAR
Single-phase loads	90 kW	-
Two-phase loads	178 kW	-
Three-phase induction motors	127 kW	72 kVAR
Three-phase induction load	-	10 kVAR

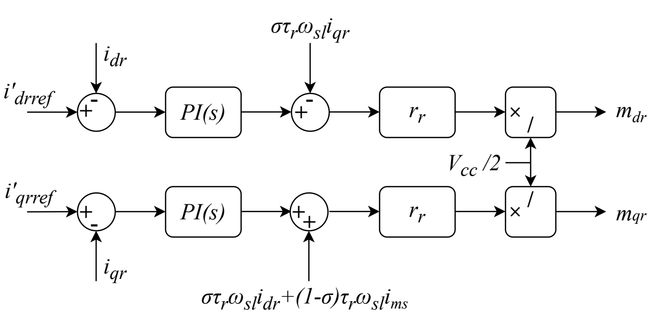

FIGURE 2. Control scheme of RSC.

of the active and reactive powers [19]. The magnetic flux estimator provides a slip angle θ_{sl} used to calculate abc to dq transform, and vice-versa, of rotor magnitude [20].

The control scheme in frequency domain is shown in Fig. 2, where σ represents the total dispersion coefficient; τ_r, the rotor time constant; ω_{sl}, the slip speed, and i_{ms}, the magnetizing current of DFIG.

B. GSC Control

The GSC control strategies are focused on regulating the DC link. In this regard, the GSC employs two control loops: an inner current loop and an outer DC bus voltage loop. The inner current loop is employed to regulate, indirectly, the active and reactive power supplied to the utility grid. Meanwhile, the outer DC bus voltage loop provides the active power reference to the inner loop.

The inner current control loop uses two control strategies, which are the Proportional Integral (PI) controller in the dq reference frame, and the Proportional multi-Resonant (PR) controller in $\alpha\beta$ reference frame [13]. The PI controller, as shown in Fig. 3a, requires utility grid synchronization for work, whereas it is unnecessary for the PR controller, Fig. 3b. Therefore, the synchronization between GSC and the utility grid is achieved applying a Phase-Locked Loop (PLL). The PLL generates angle ρ, looking for the magnitude of the quadrature axis voltage to be zero [21].

The reference currents for GSC control are based on the active and reactive power equations at each reference frame. The dynamic of the GSC current on the AC side is represented in transfer function G_f from PCC voltage to GSC current. The G_f does not depend on the frame adopted. Therefore, the transfer function, expressed in (7), can be used in both GSC control schemes.

$$G_f\left(s\right) = \frac{1}{Ls + R} \tag{7}$$

where L and R are inductance and resistance of the GSC filter.

The DC link voltage control, shown in Fig. 4, provides active power reference to the inner current control loop.

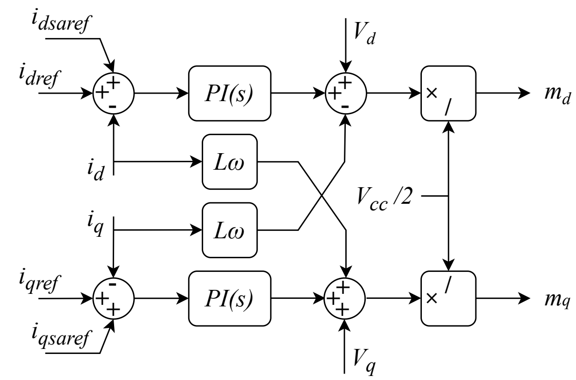

(a)

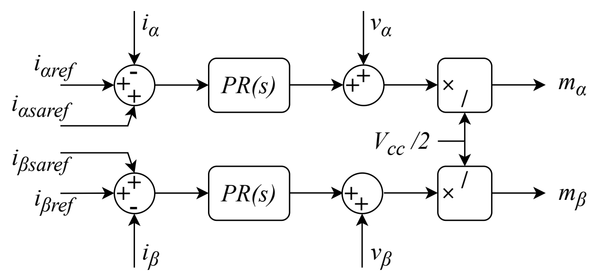

(b)

FIGURE 3. Control scheme of GSC (a) GSC with PI controller (b) GSC with PR controller.

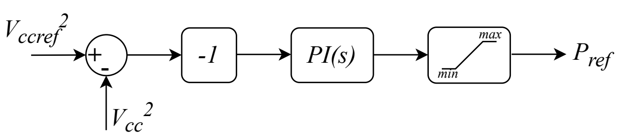

FIGURE 4. Control scheme of DC link voltage.

The dynamic of DC link voltage is represented in transfer function G_{DC} from DC link voltage squared (V_{CC}^2) to reference power (P_{ref}) by (8) [20]. The active power through the rotor affects the operation point of the DC link transfer function.

$$G_{DC}(s) = \frac{V_{CC}^2}{P_{ref}} = -\left(\frac{2}{C}\right)\frac{\tau s + 1}{s} \tag{8}$$

$$\tau = \frac{2LP_{ref0}}{3V_s^2} \tag{9}$$

where τ is a time constant of the DC link and P_{ref0} is active power at the operating point [20].

The ancillary services are provided by GSC that adds current references from the CPT application to the reference currents of GSC control.

IV. CONSERVATIVE POWER THEORY

The CPT proposes an approach in the time domain based on abc coordinates under non-sinusoidal periodic operating conditions. The necessary concepts for CPT are instantaneous active power p and instantaneous reactive energy w_r, shown in (10) and (11), respectively.

$$p(t) = \underline{v}(t) \cdot \underline{i}(t) = \sum_{\mu=1}^{3} v_\mu(t)\, i_\mu(t) \tag{10}$$

$$w_r(t) = \underline{\hat{v}}(t) \cdot \underline{i}(t) = \sum_{\mu=1}^{3} \widehat{v}_\mu(t)\, i_\mu(t) \tag{11}$$

where $\underline{v}$ and $\underline{i}$ are voltage and current vectors at a three-phase port. μ index refers to each port phase. The unbiased integrals of phase voltages $\hat{v}$ are given by the difference between the time integral and its mean value.

The corresponding average values are active power and reactive energy, which are given in (12) and (13), respectively.

$$P = \langle \underline{v}, \underline{i} \rangle = \frac{1}{T}\sum_{\mu=1}^{3}\int_0^T v_\mu(t)\, i_\mu(t) = \sum_{\mu=1}^{3} P_\mu \tag{12}$$

$$W_r = \langle \underline{\widehat{v}}, \underline{i} \rangle = \frac{1}{T}\sum_{\mu=1}^{3}\int_0^T \widehat{v}_\mu(t)\, i_\mu(t) = \sum_{\mu=1}^{3} W_{r\mu} \tag{13}$$

The CPT accomplishes an orthogonal decomposition of load phase currents as five components that are: balanced active currents $\underline{i}_a^b$, balanced reactive currents $\underline{i}_r^b$, unbalanced active currents $\underline{i}_a^u$, unbalanced reactive currents $\underline{i}_r^u$, and residual currents $\underline{i}_v$, as shown in (14) to (18) [22].

$$\underline{i}_a^b = \frac{\langle \underline{v}, \underline{i} \rangle}{\|\underline{v}\|^2}\underline{v} = \frac{P}{V^2}\underline{v} = G^b \underline{v} \tag{14}$$

$$\underline{i}_r^b = \frac{\langle \underline{\widehat{v}}, \underline{i} \rangle}{\|\underline{\widehat{v}}\|^2}\underline{\widehat{v}} = \frac{W_r}{V^2}\underline{\widehat{v}} = B^b \underline{\widehat{v}} \tag{15}$$

$$i_{a\mu}^u = \left(\frac{P_\mu}{V_\mu^2} - G^b\right) v_\mu = \left(G_\mu - G^b\right) v_\mu \tag{16}$$

$$i_{r\mu}^u = \left(\frac{W_{r\mu}}{\widehat{V}_\mu^2} - B^b\right) \widehat{v}_\mu = \left(B_\mu - B^b\right) \widehat{v}_\mu \tag{17}$$

$$\underline{i}_v = \underline{i} - \underline{i}_a^b - \underline{i}_r^b - \underline{i}_a^u - \underline{i}_r^u \tag{18}$$

where B_μ and B^b are phase and balanced equivalent reactivity, respectively. G_μ and G^b are phase and balanced equivalent conductance, respectively.

A. Power Terms

The three-phase current is represented as the sum of the components of the CPT, shown in (19).

$$\underline{i} = \underline{i}_a^b + \underline{i}_r^b + \underline{i}_a^u + \underline{i}_r^u + \underline{i}_v \tag{19}$$

The components are orthogonal. Thus, the Euclidean norm is shown in (20).

$$I^2 = I_a^{b\,2} + I_r^{b\,2} + I_a^{u\,2} + I_r^{u\,2} + I_v^{\,2} \tag{20}$$

The apparent power (A) is represented in (21) based on (20).

$$A^2 = P^2 + Q^2 + U_a^2 + U_r^2 + D^2 \tag{21}$$

$$P = V I_a^b \tag{22}$$

$$Q = VI_r^b \tag{23}$$

$$U = \sqrt{U_a^2 + U_r^2} = \sqrt{(VI_a^u)^{\ 2} + (VI_r^u)^{\ 2}} \tag{24}$$

$$D = VI_v \tag{25}$$

where P is the active power, Q is the reactive power, U is the unbalanced power, and D is a the void power [22].

B. CPT application for ancillary services

The orthogonal decomposition current in (26) is employed as a reference signal to GSC control for providing ancillary services [23]. Current components employed in the reference signal are: the unbalanced active currents, the balanced and unbalanced reactive currents, and the residual current.

$$\underline{i}_{saref} = \underline{i}_a^u + \underline{i}_r^b + \underline{i}_r^u + \underline{i}_v \tag{26}$$

The reference signals are transformed into dq and $\alpha\beta$ reference frames depending on the reference frame at the control scheme.

V. POWER QUALITY INDICATORS

The performances of ancillary services are analyzed by employing power quality indicators. Each indicator is related to one of the three ancillary services in this research. The indicators presented in this work include standard and CPT power quality indicators. Standard power quality indicators are based on standards such as IEEE standards and PRODIST. Meanwhile, the CPT factors are considered to CPT power quality indicators.

A. Standard power quality indicators

The active filtering service is analyzed using Total Harmonic Distortion (THD) and Total Rated-Current Distortion (TRD). Both indicators are related to harmonic distortion. The THD, defined in IEEE 519 standard, is calculated employing the harmonics components until the 50$^{\text{th}}$-order of the fundamental frequency, shown in (27) [24]. Meanwhile, the TRD, defined in IEEE 1547 and IEEE 1459 standard, considers the inter-harmonics in the calculation of total distortion, shown in (28) [25], [26].

$$THD = \frac{\sqrt{\sum_{n=2}^{50} I_n^2}}{I_1} 100\,\% \tag{27}$$

$$TRD = \frac{\sqrt{I^2 - I_1^2}}{I_1} 100\,\% \tag{28}$$

where I_1 is the fundamental magnitude of harmonic spectrum. I_n is the n-th harmonic component of the current in the PCC.

The reactive power compensation and the unbalanced phase compensation services are analyzed employing the power factor (PF), in (29), and the current unbalanced phase factor (K_c), in (30), respectively. These indicators are based on the Brazilian standard PRODIST [27].

$$FP = \frac{P}{\sqrt{P^2 + Q^2}} \tag{29}$$

$$K_c = \frac{I_-}{I_+} 100\,\% \tag{30}$$

where P and Q are the active and reactive power through the PCC, respectively. I_+ and I_- are the magnitude root-mean-square current of positive and negative sequences from symmetrical components.

The limits for these indicators consider the IEEE 519 standard and PRODIST, shown in Table 2. The harmonic distortion and power factor are limited in these standards. However, these standards do not define the limits of K_c. Therefore, the limit of voltage unbalanced phase factor from PRODIST is considered to be K_c limits. These limits are considered during PCC nominal conditions.

TABLE 2. Limits of standard power quality indicators

Indicator	Min	Max
THD	-	5 %
PF	0.92	1
K_c	-	3 %

B. CPT power quality indicators

The CPT formulation provides indicators that characterize the electric system, as shown in (31) to (34).

$$\lambda = \frac{P}{A} = \frac{P}{\sqrt{P^2 + Q^2 + U^2 + D^2}} \tag{31}$$

$$\lambda_Q = \frac{Q}{\sqrt{P^2 + Q^2}} \tag{32}$$

$$\lambda_U = \frac{U}{\sqrt{P^2 + Q^2 + U^2}} \tag{33}$$

$$\lambda_D = \frac{D}{A} \tag{34}$$

where λ is the global conformity factor, λ_Q is the reactivity factor, λ_U is the asymmetry factor, and λ_D is the distortion factor.

Each indicator is related to three ancillary services. The global conformity factor is related to the active power of the electric system. The reactivity factor is associated with energy storage elements and the phase difference between current and voltage. The asymmetry factor arises when the system exhibits unbalanced loads. Finally, the distortion factor is related to the distortions of currents concerning the waveform of the produced voltage, for example, by non-linear loads.

VI. RESULTS

The dynamic of a WECS is simulated using *Matlab/Simulink*. The simulation type is discrete with sample time for discretization of 5 µs. The simulation parameters are detailed in the APPENDIX. The rotor angular speed varies the active power through the back-to-back converter. Therefore, the value of the electric angular speed of the rotor

TABLE 3. Analyzed cases of wind system

Case	Time interval	Ancillary service	Stator active power	Rotor Angular speed
Case 1	0.8 s to 1 s	No	0 kW	120 rad/s
Case 2	1.2 s to 1.4 s	Yes	0 kW	120 rad/s
Case 3	1.8 s to 2 s	Yes	700 kW	88 rad/s
Case 4	2.4 s to 2.6 s	Yes	700 kW	163 rad/s

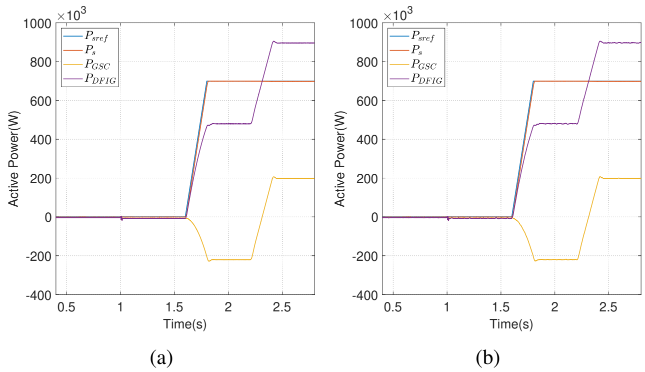

FIGURE 5. Active power in DFIG (a) GSC with PI controller (b) GSC with PR controller.

is $\pm30\,\%$ of the angular speed of the utility grid. The standard indicators are calculated from the PCC current over a measurement window of 12 cycles, which lasts $0.2\,\mathrm{ms}$. Since the DFIG speed dynamic is slower than the measurement window, the speed is assumed to remain constant throughout the measurement period.

The WECS simulation operates in four cases, detailed in Table 3. Two GSC control strategies, PI (dq reference frame) and PR ($\alpha\beta$ reference frame), are analyzed in each case. In case 1, WECS does not provide any ancillary services, whereas, in case 2, it does. In both cases 1 and 2, the system operates without active power supply to compare the performance of ancillary services in both control strategies. In cases 3 and 4, the system operates by supplying active power to the load in addition to ancillary services. Although the active power supply depends on the angular speed of the rotor, the reference for active power supplied by the stator is set at $700\,\mathrm{kW}$. In case 3, the mechanic angular speed of the rotor is $88\,\mathrm{rad/s}$, whereas, in case 4, the reference is $163\,\mathrm{rad/s}$.

Fig. 5 shows the active power in the stator, P_s, and in GSC, P_{GSC}, as well as the total active power of DFIG, P_{DFIG}, for GSC with PI controller (a) and PR controller (b). The stator active power follows the reference signal P_{sref} for both two control strategies, even though the active power through GSC exhibits varying values. The active power at output GSC varies depending on the rotor angular speed, as shown in cases 3 and 4. The system can supply active power and follow the reference, while providing the ancillary services.

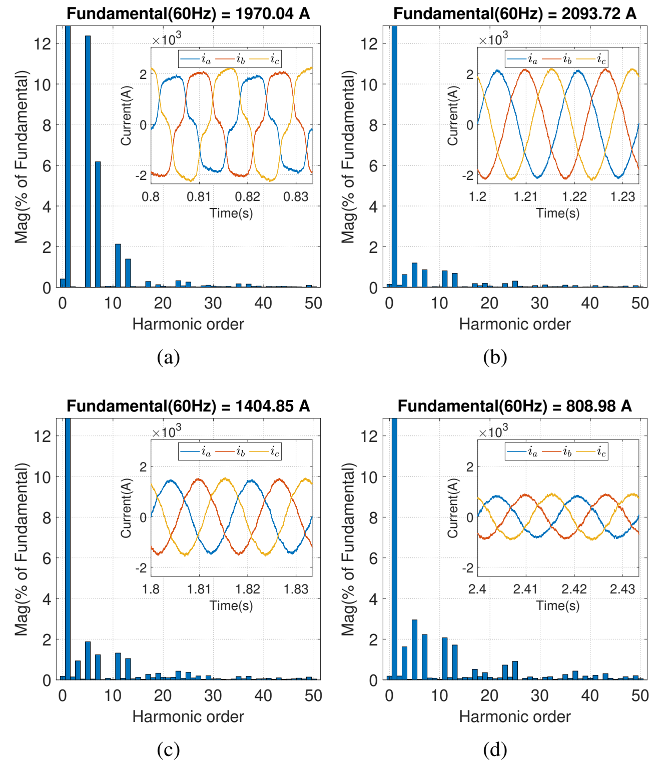

FIGURE 6. Harmonic spectrum and waveform of PCC current for GSC with PI controller (a) Case 1 (b) Case 2 (c) Case 3 (d) Case 4.

Fig. 6 and Fig. 7 depict the harmonic spectrum and waveform of PCC current in each case using both control strategies. The harmonic spectrum contains harmonic order up to 50^{th} of a single current phase. The non-linear load current predominantly exhibits 5^{th}, 7^{th}, 11^{th}, and 13^{th} order harmonics, shown in case 1 for both control strategies.

A. GSC with PI controller

In case 1, the ancillary services are inactive, resulting in unbalanced and distorted phases in the PCC currents, as shown in Fig. 6a. In this harmonic spectrum, the 5^{th} order harmonic, at $12.37\,\%$, has the highest relative magnitude. The ancillary services reduce the harmonics in cases 2 to 4, with the 5^{th} order harmonic reaching the maximum relative magnitude of $2.95\,\%$ in case 4. Similarly, the 7^{th}, 11^{th}, and 13^{th} harmonics exhibit a decrease from case 1 to case 2 to 4. The PCC currents show approximately sinusoidal balanced waveforms in cases 2 to 4. The magnitudes relative to the fundamental increases when the system supplies active power. Therefore, the harmonics show a relative magnitude increasing in cases 3 and 4.

The standard power quality indicators of PCC current are presented in Table 4. In case 1, the THD and TRD exceed $14\,\%$, surpassing the $5\,\%$ limit. The ancillary services operating in cases 2 to 4 reduce the harmonic distortion indicators. Case 2 exhibits the lowest values for THD and TRD among the cases. However, in cases 3 and 4, the supply

TABLE 4. Standard Indicators of PCC current in GSC with PI controller.

Indicators	Case 1	Case 2	Case 3	Case 4
THD	$14.07\,\%$	$2.01\,\%$	$3.09\,\%$	$5.1\,\%$
TRD	$14.14\,\%$	$2.37\,\%$	$3.73\,\%$	$6.17\,\%$
PF	0.9893	1	1	1
K_c	$6.64\,\%$	$0.63\,\%$	$0.89\,\%$	$1.43\,\%$

TABLE 5. Standard Indicators of PCC current in GSC with PR controller.

Indicators	Case 1	Case 2	Case 3	Case 4
THD	$14.06\,\%$	$0.9\,\%$	$1.45\,\%$	$2.31\,\%$
TRD	$14.13\,\%$	$1.54\,\%$	$2.54\,\%$	$4.19\,\%$
PF	0.9895	1	0.9999	0.9999
K_c	$6.62\,\%$	$0.42\,\%$	$0.57\,\%$	$0.99\,\%$

of active power reduces the fundamental magnitude of the PCC current, thereby increasing both THD and TRD.

The power factor is 0.9893 in case 1, without supplying the ancillary services. This value approaches the unitary power factor in cases 2 to 4. In case 2, the power factor remains within the limits defined by PRODIST. Note that the unitary power factor is maintained when the GSC supplies various levels of active power in cases 3 to 4.

The current unbalanced phase factor exceeds the $3\,\%$ limit in case 1, whereas it remains within the limit in cases 2. The ancillary services decrease the K_c value. However, supplying active power at PCC increases the K_c from $0.63\,\%$ in case 2 to $1.43\,\%$ in case 4.

B. GSC with PR controller

In case 1, the PCC current is predominantly composed of non-linear and unbalanced load currents, as shown in Fig. 7a. The harmonic spectrum in cases 2 to 4 demonstrates a significant reduction in the 5$^{\text{th}}$, 7$^{\text{th}}$, 11$^{\text{th}}$, and 13$^{\text{th}}$ order harmonics. The 5$^{\text{th}}$ harmonic exhibits the highest magnitude among the harmonics in case 1, decreasing from $12.35\,\%$ to a maximum of $0.61\,\%$ in case 4. In Fig. 7d, the 3$^{\text{rd}}$ order harmonic, at $1.51\,\%$, represents the highest relative magnitude in case 4.

For this control strategy, the standard indicators of PCC current are exhibited in Table 5. In case 1, the THD and TRD exceed the $5\,\%$ limit. Meanwhile, the harmonic distortion indicators in cases 2 remain within the limit. In case 2, the THD and TRD present the lowest values.

The PCC current has a PF of 0.9895 in case 1. In case 2, the PF approaches the unitary power factor. In cases 3 and 4, the power factor is nearly equal to 1, so it is considered a unitary power factor.

In case 1, the current unbalanced phase factor is $6.62\,\%$, exceeding the $3\,\%$ limit. In cases 2 to 4, the K_c is below $1\,\%$. The K_c of $0.99\,\%$ in case 4 is higher than $0.42\,\%$ in case 2 due to the active power injected at the PCC.

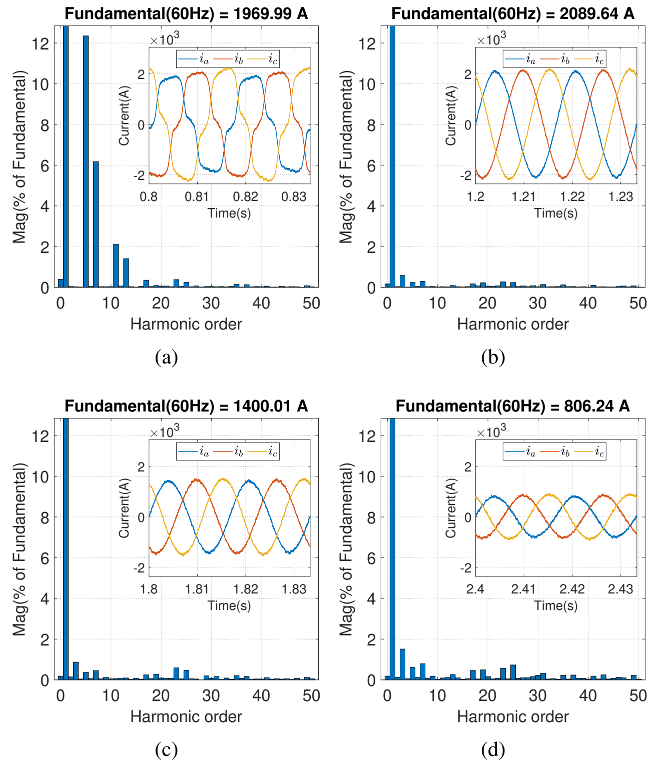

FIGURE 7. Harmonic spectrum and waveform of PCC current for GSC with PR controller (a) Case 1 (b) Case 2 (c) Case 3 (d) Case 4.

C. Comparison between two control strategies

The distortion and unbalanced phase current in case 1 is compensated by ancillary services in cases 2 to 4. The harmonic spectrum exhibits a reduction in 5$^{\text{th}}$, 7$^{\text{th}}$, 11$^{\text{th}}$, and 13$^{\text{th}}$ harmonic orders when ancillary services are active. The GSC with PR controller reduces the magnitude of these harmonics more effectively compared to GSC with PI controller. Supplying active power by the system decreases the fundamental component of the PCC current harmonic spectrum. Thus, the distortion harmonic in case 2 presents a lower value than in cases 3 and 4.

The THD is lower than TRD due to the non-consideration of inter-harmonics in calculation. The limits of standard power quality indicators are checked in cases 1 and 2 when the PCC presented nominal current condition. The THD and TRD decrease to values below than $5\,\%$ limit from case 1 to case 2. The reactive power compensation and active filtering are related to the PF value. The GSC with PR controller presents better indicator values than GSC with PI controller.

The CPT indicators for GSC with PI and PR controllers are exhibited in Table 6 and Table 7, respectively. The standards do not employ the CPT indicators for characterise the electrical system, so the limits of CPT indicators are not defined. The distortion factor, λ_D, of the CPT indicators exhibits a correlation with harmonic distortion. In case 1, the λ_D is lower than the standards harmonic distortions. However, in the others cases, when the ancillary services

TABLE 6. CPT Indicators of PCC current for GSC with PI controller.

Indicators	Case 1	Case 2	Case 3	Case 4
λ_D	0.1298	0.0291	0.0406	0.0614
λ	0.9785	0.9992	0.9984	0.996
λ_Q	0.146	0.0005	0.0012	0.0008
λ_U	0.0708	0.0259	0.0382	0.065

TABLE 7. CPT Indicators of PCC current for GSC with PR controller.

Indicators	Case 1	Case 2	Case 3	Case 4
λ_D	0.1296	0.0233	0.031	0.0447
λ	0.9786	0.9994	0.9987	0.9969
λ_Q	0.1451	0.0018	0.012	0.0103
λ_U	0.0707	0.0255	0.0376	0.0638

are active, it is higher. In these cases, its value is closer to TRD than THD.

The global conformity factor, λ, and PF are correlated due the similarity of their calculation. The λ is lower than PF since its calculation considers the unbalanced and void power. Therefore, the λ value is not unitary. The λ in the GSC with both two controllers does not exhibit a significant difference. The reactivity factor, λ_Q, is related to the reactive power in the PCC, so its value is close to zero when the ancillary services are active.

In case 4, the asymmetry factor, λ_U, is around 0.06, which is close to the value of 0.07 in case 1. Therefore, the λ_U does not correspond to the K_c for all cases.

VII. CONCLUSION

This paper presented a DFIG power plant incorporates three types of ancillary services simultaneously. The CPT was used to provide three type of services: active filtering, reactive power compensation, and unbalanced phase compensation. Furthermore, two control strategies in the dq reference frame and $\alpha\beta$ reference frame used in back-to-back converter were compared. The CPT orthogonal decomposition current was employed as a reference signal to GSC control for providing three services. The GSC provided ancillary services in addition to injecting and absorbing active power.

The non-linear load current predominantly exhibits the 5^{th}, 7^{th}, 11^{th}, and 13^{th} harmonic order, which are compensated by ancillary services using the GSC with PI and PR controller. The GSC with the PR controller exhibits lower harmonic distortion and K_c than that with the PI controller. Furthermore, it presented a unitary power factor when the ancillary services are active. The limits of standard power quality indicators were checked in cases when the PCC presented nominal current condition. The standard power quality indicators remain within their limits for the GSC with PR and PI controller.

The standard power quality indicators, as well as λ_D and λ, characterized the PCC current. The λ_D and the λ were correlated with the harmonic distortion and power factor, respectively. Nevertheless, the λ_U was not exhibit a correlation with K_c. This work focused on simulating the ancillary services on a $1.5\,\mathrm{MW}$ power plant. The next step will involve experimentally validating the control strategies and ancillary services on a smaller-scale power system, which is under development for future studies.

APPENDIX

Utility grid parameters: $575\,\mathrm{V}$, $60\,\mathrm{Hz}$, $r_g = 0.01\,\mathrm{m\Omega}$, $L_g = 2.85\,\mathrm{\mu H}$.

DFIG parameters: $1.5\,\mathrm{MW}$, $575\,\mathrm{V}$, $60\,\mathrm{Hz}$, $r_s = 1.4\,\mathrm{m\Omega}$, $r'_r = 0.99\,\mathrm{m\Omega}$, $L_s = 89.98\,\mathrm{\mu H}$, $L_r = 82.08\,\mathrm{\mu H}$, $L_m = 1.526\,\mathrm{mH}$, $p = 6$.

DC link capacitor: $C_e = 10\,\mathrm{mF}$.

GSC inductive filter: $R = 8.8\,\mathrm{m\Omega}$, $L = 125\,\mathrm{\mu H}$.

ACKNOWLEDGMENT

Authors acknowledges the support from FAPESP (grant no. 2017/11986-5) and Shell and the strategic importance of the support provided by ANP (Brazil's National Oil, Natural Gas, and Biofuels Agency). This study was financed in part by the Coordenação de Aperfeiçoamento de Pessoal de Nível Superior – Brasil (CAPES) and the Conselho Nacional de Desenvolvimento Científico e Tecnológico (CNPq) (grants 402983/2021-1, 308589/2022-0 and 408529/2023-7). In addition, the authors are grateful to all collaborators from the Universidade Estadual de Campinas (UNICAMP). Acknowledgments are extended to the School of Electrical and Computer Engineering (FEEC).

AUTHOR'S CONTRIBUTIONS

HINOSTROZA, C. L. A.: Conceptualization, Data Curation, Formal Analysis, Investigation, Methodology, Software, Validation, Visualization, Writing – Original Draft. **SILVEIRA, J. P. C.**: Conceptualization, Formal Analysis, Methodology, Project Administration, Supervision, Visualization, Writing – Review & Editing. **DE PAULA, M. V.**: Formal Analysis, Methodology, Supervision, Visualization, Writing – Review & Editing. **DOS SANTOS NETO, P. J.**: Formal Analysis, Funding Acquisition, Methodology, Supervision, Visualization, Writing – Review & Editing. **RUPPERT FILHO, E.**: Conceptualization, Funding Acquisition, Project Administration, Resources, Supervision. **BARROS, T. A. S.**: Funding Acquisition, Methodology, Project Administration, Resources, Supervision, Writing – Review & Editing.

PLAGIARISM POLICY

This article was submitted to the similarity system provided by Crossref and powered by iThenticate – Similarity Check.

REFERENCES

[1] K. Oureilidis, K.-N. Malamaki, K. Gallos, A. Tsitsimelis, C. Dikaiakos, S. Gkavanoudis, M. Cvetkovic, J. M. Mauricio, J. M. Maza Ortega, J. L. M. Ramos, G. Papaioannou, C. Demoulias, "Ancillary Services Market Design in Distribution Networks: Review and Identification of Barriers", *Energies*, vol. 13, no. 4, 2020, doi:10.3390/en13040917.

[2] M. Bajaj, A. K. Singh, "Grid integrated renewable DG systems: A review of power quality challenges and state-of-the-art mitigation techniques", *International Journal of Energy Research*, vol. 44, no. 1, pp. 26–69, 2020, doi:10.1002/er.4847.

[3] M. Debouza, A. Al-Durra, "Grid Ancillary Services From Doubly Fed Induction Generator-Based Wind Energy Conversion System: A Review", *IEEE Access*, vol. 7, pp. 7067–7081, 2019, doi:10.1109/ACCESS.2018.2890168.

[4] M. A. Basit, S. Dilshad, R. Badar, S. M. Sami ur Rehman, "Limitations, challenges, and solution approaches in grid-connected renewable energy systems", *International Journal of Energy Research*, vol. 44, no. 6, pp. 4132–4162, 2020, doi:10.1002/er.5033.

[5] G. Todeschini, A. Emanuel, "Wind energy conversion systems as active filters: design and comparison of three control methods", *IET Renewable Power Generation*, vol. 4, pp. 341–353(12), July 2010, doi:10.1049/iet-rpg.2009.0147.

[6] M. Boutoubat, L. Mokrani, M. Machmoum, "Control of a wind energy conversion system equipped by a DFIG for active power generation and power quality improvement", *Renewable Energy*, vol. 50, pp. 378–386, 2013, doi:10.1016/j.renene.2012.06.058.

[7] C. L. A. Hinostroza, J. P. C. Silveira, T. A. dos Santos Barros, M. V. de Paula, P. J. dos Santos Neto, E. R. Filho, "Proposal of WECS Technology with DFIG Using Conservative Power Theory for Ancillary Services", *in 2023 IEEE 8th Southern Power Electronics Conference and 17th Brazilian Power Electronics Conference (SPEC/COBEP)*, pp. 1–7, 2023, doi:10.1109/SPEC56436.2023.10408501.

[8] A. B. Moreira, T. A. D. S. Barros, V. S. D. C. Teixeira, R. R. D. Souza, M. V. D. Paula, E. R. Filho, "Control of Powers for Wind Power Generation and Grid Current Harmonics Filtering From Doubly Fed Induction Generator: Comparison of Two Strategies", *IEEE Access*, vol. 7, pp. 32703–32713, 2019, doi:10.1109/ACCESS.2019.2899456.

[9] T. Mesbahi, A. Ouari, T. Ghennam, E. M. Berkouk, N. Mesbahi, "A hybrid wind energy conversion system/active filter for non linear conditions", *International Journal of System Assurance Engineering and Management*, vol. 7, no. S1, p. 1–8, Mar. 2014, doi:10.1007/s13198-014-0250-5.

[10] T. Mesbahi, T. Ghennam, E. M. Berkouk, "Control of a Wind Energy Conversion System with active filtering function", *in 2011 International Conference on Power Engineering, Energy and Electrical Drives*, pp. 1–6, 2011, doi:10.1109/PowerEng.2011.6036441.

[11] E. Tremblay, S. Atayde, A. Chandra, "Direct power control of a DFIG-based WECS with active filter capabilities", *in 2009 IEEE Electrical Power & Energy Conference (EPEC)*, pp. 1–6, 2009, doi:10.1109/EPEC.2009.5420770.

[12] A. Gaillard, P. Poure, S. Saadate, M. Machmoum, "Variable speed DFIG wind energy system for power generation and harmonic current mitigation", *Renewable Energy*, vol. 34, no. 6, pp. 1545–1553, 2009, doi:10.1016/j.renene.2008.11.002.

[13] R. R. Souza, A. B. Moreira, T. A. Barros, E. Ruppert, "A proposal for a wind system equipped with a doubly fed induction generator using the Conservative Power Theory for active filtering of harmonics currents", *Electric Power Systems Research*, vol. 164, pp. 167–177, 2018, doi:10.1016/j.epsr.2018.07.027.

[14] S. Puchalapalli, B. Singh, S. K. Tiwari, P. K. Goel, "Design and Analysis of Grid-Interactive DFIG Based WECS for Regulated Power Flow", *IEEE Transactions on Industry Applications*, vol. 56, no. 5, pp. 5396–5407, 2020, doi:10.1109/TIA.2020.3011059.

[15] M. Boutoubat, L. Mokrani, A. Zegaoui, "Power quality improvement by controlling the Grid Side Converter of a wind system based on a DFIG", *in 2017 6th International Conference on Systems and Control (ICSC)*, pp. 360–365, 2017, doi:10.1109/ICoSC.2017.7958675.

[16] R. R. de Souza, A. B. Moreira, T. A. S. Barros, E. Ruppert, "Conservative power theory: application in a wind system with DFIG to compensate harmonic currents and unbalance electric current", *Renewable Energy and Power Quality Journal*, vol. 1, p. 247–252, Apr. 2018, doi:10.24084/repqj16.275.

[17] G. Todeschini, "Wind Energy Conversion Systems as active filters under unbalanced load conditions", *in Proceedings of 14th International Conference on Harmonics and Quality of Power - ICHQP 2010*, pp. 1–7, 2010, doi:10.1109/ICHQP.2010.5625458.

[18] F. Blaabjerg, D. Xu, W. Chen, N. Zhu, *Advanced Control of Doubly Fed Induction Generator for Wind Power Systems*, John Wiley & Sons, Inc., 2018, doi:10.1002/9781119172093.

[19] E. Bim, *Máquinas elétricas e acionamento*, 4 ed., Elsevier, 2018.

[20] A. Yazdani, R. Iravani, *Voltage-sourced converters in power systems*, Wiley - IEEE, Wiley-Blackwell, Hoboken, NJ, Mar. 2010.

[21] W. Liu, F. Blaabjerg, "Chapter 10 - Phase-locked loops and their design", *in* F. Blaabjerg, ed., *Control of Power Electronic Converters and Systems*, pp. 269–301, Academic Press, 2021, doi:10.1016/B978-0-12-819432-4.00013-5.

[22] P. Tenti, H. K. M. Paredes, P. Mattavelli, "Conservative Power Theory, a Framework to Approach Control and Accountability Issues in Smart Microgrids", *IEEE Transactions on Power Electronics*, vol. 26, no. 3, pp. 664–673, 2011, doi:10.1109/TPEL.2010.2093153.

[23] T. D. C. Busarello, A. Mortezaei, A. Péres, M. G. Simões, "Application of the Conservative Power Theory Current Decomposition in a Load Power-Sharing Strategy Among Distributed Energy Resources", *IEEE Transactions on Industry Applications*, vol. 54, no. 4, pp. 3771–3781, 2018, doi:10.1109/TIA.2018.2820641.

[24] IEEE, "IEEE Recommended Practice and Requirements for Harmonic Control in Electric Power Systems", *IEEE Std 519-2014 (Revision of IEEE Std 519-1992)*, pp. 1–29, 2014, doi:10.1109/IEEESTD.2014.6826459.

[25] IEEE, "IEEE Standard for Interconnection and Interoperability of Distributed Energy Resources with Associated Electric Power Systems Interfaces", *IEEE Std 1547-2018 (Revision of IEEE Std 1547-2003)*, pp. 1–138, 2018, doi:10.1109/IEEESTD.2018.8332112.

[26] IEEE, "IEEE Standard Definitions for the Measurement of Electric Power Quantities Under Sinusoidal, Nonsinusoidal, Balanced, or Unbalanced Conditions", *IEEE Std 1459-2010 (Revision of IEEE Std 1459-2000)*, pp. 1–50, 2010, doi:10.1109/IEEESTD.2010.5439063.

[27] ANEEL, "Procedimentos de distribuição de energia elétrica no sistema elétrico nacional - PRODIST Módulo 8 - Qualidade da Energia Elétrica", Agência Nacional de Energia Elétrica, 2021.

BIOGRAPHIES

Carlos Leonardo Ancasi Hinostroza received the B.S. degree in electronic engineering from National University of Engineering, Lima, Perú, in 2018, and M.S. degree in electrical engineering from University of Campinas (UNICAMP), Campinas, Brazil, in 2022. He is currently pursuing the Ph.D. degree from the University of Campinas, Campinas, Brazil. He involves in the areas of power electronic and electrical machines. His research interests include renewable energy and power quality.

João Pedro Carvalho Silveira received the B.S. degree in energy engineering, in 2013, and M.S. degree in electrical engineering, in 2016, both from the University of Brasilia (UnB), Brasilia, Brazil. He received the Ph.D. degree in the University of Campinas (UNICAMP), Campinas, Brazil, at the Power Electronics Laboratory (LEPO). He is currently as collaborator professor in School Electrical and Computer Engineering, UNICAMP, and postdoctoral researcher in the LEPO. He works in the areas of power electronics applications and electrical drives. His research interests include microgrids, renewable energy, photovoltaic systems, energy storage systems, reliability assessment, power quality, and machine driving.

Marcelo Vinícius de Paula received the B.S. degree in electrical engineering from the Federal University of Goiás, Brazil, in 2016, the M.Sc. degree in electrical engineering from University of Campinas (UNICAMP), Campinas, Brazil, in 2018, and Ph.D. in mechatronics engineering from UNICAMP, Campinas, Brazil, 2022. Currently, he is a Professor at Faculty of Mechanical Engineering of UNICAMP. He involves in the areas of electric machines and drives, power electronics, and transportation electrification. His research interests include renewable energy, electric machine drives and electric vehicles.

Pedro José dos Santos Neto received the B.S. degree in electrical engineering from the Federal University of Vale do Sao Francisco (UNIVASF), Petrolina, Brazil, in 2016, the M.S. degree from the University of Campinas (UNICAMP), Campinas, Brazil, in 2017, and the Ph.D. degree from UNICAMP, in 2021, under the São Paulo Research Foundation (FAPESP) Scholarship Program. In 2019, he was a Guest Ph.D. Visitor with the Center for Research on Microgrids (CROM), Aalborg University, Aalborg East, Denmark. He is currently a Professor with the Mechanical Engineering Faculty, UNICAMP. He works in the areas of microgrids, electrical machines, and power electronics. His research interests include DC microgrids, Wind Systems, and vehicle electrification. He is a member of the IEEE and the Brazilian Society of Power Electronics (SOBRAEP).

Ernesto Ruppert Filho received the B.S. degree in electrical engineering and the M.S. and Ph.D. degrees from the University of Campinas (UNICAMP), Campinas, Brazil, in 1971, 1974, and 1983, respectively. From 1972 to 1978, he was with the Electrical and Computer Engineering School, UNICAMP, as an Assistant Professor of electromechanical energy conversion. From 1979 to 1983, he was with General Electric, Brazil, designing large induction and synchronous motors and working as an Application Engineer dedicated to large motors and generators. He is currently a Full Professor with the Electrical and Computer Engineering School, UNICAMP, researching and teaching in the areas of electrical machines, power electronics, drives, and electrical power systems.

Tárcio André dos Santos Barros received the B.S. degree in electrical engineering from the Federal University of Vale do São Francisco (UNIVASF), Petrolina, Brazil, in 2010, and the M.S. and Ph.D. degrees from the University of Campinas (UNICAMP), Campinas, Brazil, in 2012 and 2015, respectively. From 2016 to 2017, he was a Researcher with the Power Electronics Laboratory (LEPO), University of Campinas, under the FAPESP Postdoctoral Program. He is currently a Professor with the Electrical and Computer Engineering Faculty, UNICAMP, and the Coordinating Member of the Brazilian Government Program ROTA 2030-FUNDEP (biofuel, vehicle safety, and alternative propulsion systems to combustion). He works in the areas of electrical machines, power electronics, electrical vehicles, and electrical drives. His research interests include machine drives, switched reluctance machines, doubly fed induction generators, and solar energy. He is a member of the Brazilian Society of Power Electronics (SOBRAEP).